

Accretion onto the Supermassive Black Hole in M87

Tiziana Di Matteo^{1,2,3}, Steven W. Allen⁴, Andrew C. Fabian⁴, Andrew S. Wilson⁵, Andrew J. Young⁵

ABSTRACT

Chandra X-ray observations of the giant elliptical galaxy M87 resolve the thermal state of the hot interstellar medium into the accretion (Bondi) radius of its central $3 \times 10^9 M_\odot$ black hole. We measure the X-ray gas temperature and density profiles and calculate the Bondi accretion rate, $\dot{M}_{\text{Bondi}} \sim 0.1 M_\odot \text{yr}^{-1}$. The X-ray luminosity of the active nucleus of M87 observed with *Chandra* is $L_{x,0.5-7 \text{ keV}} \sim 7 \times 10^{40} \text{ erg s}^{-1}$. This value is much less than the predicted nuclear luminosity, $L_{\text{Bondi}} \sim 5 \times 10^{44} \text{ erg s}^{-1}$, for accretion at the Bondi rate with a canonical accretion radiative efficiency of 10%. If the black hole in M87 accretes at this rate it must do so at a much lower radiative efficiency than the canonical value. The multiwavelength spectrum of the nucleus is consistent with that predicted by an advection-dominated flow. However, as is likely, the X-ray nucleus is dominated by jet emission then the properties of flow must be modified, possibly by outflows. We show that the overall energetics of the system are just consistent with the predicted Bondi nuclear power. This suggests that either most of the accretion energy is released in the relativistic jet or that the central engine of M87 undergoes on-off activity cycles. We show that, at present, the energy dumped into the ISM by the jet may reduce the accretion rate onto the black hole by a factor $\propto (v_j/c_s)^{-2}$, where v_j is the jet velocity and c_s the ISM sound speed, and that this is sufficient to account for the low nuclear luminosity.

Subject headings: accretion, accretion disks — black hole physics — galaxies:individual (M87) — X-rays: galaxies

1. Introduction

The nucleus of M87 (NGC 4486) contains a black hole of mass $M \sim 3 \times 10^9 M_\odot$ directly determined from *HST* observations (Ford et al. 1995; Harms et al. 1995; Macchetto et al. 1997).

¹Harvard-Smithsonian Center for Astrophysics, 60 Garden St., Cambridge, MA 02138

²Max-Planck-Institute für Astrophysik, Karl-Schwarzschild-Str. 1, 85740 Garching bei München, Germany

³Carnegie-Mellon University, Dept. of Physics, 5000 Forbes Ave., Pittsburgh 15231

⁴Institute of Astronomy, Madingley Road, Cambridge, CB3 0HA, UK

⁵Astronomy Department, University of Maryland, College Park, MD 20742

It is a nearby active nucleus with a one sided jet and large-scale radio structure. However, the activity displayed by its nucleus is far less than what is predicted if the central black hole were accreting mass from its hot interstellar medium (with a standard radiative efficiency of ~ 10 per cent; see e.g. Fabian & Rees 1995; Reynolds et al. 1996; Di Matteo et al. 2000). M87 is probably the most illustrative case of a low-luminosity system otherwise common in nearby galaxies known to contain supermassive black holes (e.g, Magorrian et al. 1998; Ferrarese & Merritt 2000).

There are two possible explanations for the low luminosities of nearby black holes: (a) the accretion occurs at extremely low rates or (b) the accretion occurs at low radiative efficiencies as predicted, for example, by advection dominated accretion flow models (ADAFs; e.g. Rees et al. 1982; Narayan & Yi 1994,1995; Abramowicz et al. 1995 but see also inflow-outflow models; e.g. Blandford & Begelmann 1999; Stone et al. 1999; or CDAFs; e.g. Quataert & Gruzinov 2002). In order to discriminate between these two possibilities, it is necessary to determine both the accretion rates and the nuclear luminosities precisely. Direct measurement of the latter and evaluation of the former has not been possible with previous X-ray satellites. Here, we show that, for the nucleus of M87, both can now be achieved with *Chandra*.

The massive black holes at the center of elliptical galaxies are likely to accrete primarily from the surrounding hot, quasi-spherical ISM. Accretion rates can therefore be simply estimated using Bondi accretion theory. This requires accurate measurements of both the density and temperature of the hot, X-ray emitting ISM at the 'Bondi accretion radius', the radius at which the gravitational potential of the central black hole begins to dominate the dynamics of the hot gas and the gas starts to fall into the black hole.

Thanks to its high spatial resolution and sensitivity, the *Chandra X-ray Observatory* is able to provide some of the most stringent constraints on the properties of low-luminosity black holes. In particular, at the distance of M87 (18 Mpc), the spatial resolution of *Chandra* corresponds to a radius of less than a hundred parsec or, equivalently, a few 10^5 Schwarzschild radii. For M87, this allows us to measure, for the first time, fundamental properties of the ISM *at the accretion radius* of the black hole, and thereby estimate the mass supply into the accretion flow.

2. Gas properties at the black hole accretion radius

2.1. Central temperature and density

Details of the *Chandra* observations and observing strategy are presented by Wilson & Yang (2002). In brief, M87 was observed twice with *Chandra*, on 2000 July 29 and 2000 July 30. Both observations were carried out using the Advanced CCD Imaging Spectrometer (ACIS) and back-illuminated S3 detector. The first observation was made in a full-frame mode with a 3.2 frame time. The net exposure time, after removing periods associated with small background flares, was 33.7ks. These data have been used to study the properties of the diffuse X-ray gas in

M87. The second, shorter observation was made in a reduced 1/8 sub-array mode with a frame time of 0.4s. The use of this mode avoids problems associated with pile-up in the data for the brightest knots of the jet and the central AGN (Wilson & Yang 2002). The exposure time for the second observation was 12.8ks. High resolution *Chandra* images and detailed analyses of the jet and cluster properties are presented by Wilson & Yang (2002) and Young, Wilson & Mundell (2002), respectively.

Spectra were extracted from five circular annuli centered on the nucleus (Figure 1). The data for the innermost region, which has a radius of 4 detector pixels (approximately 2 arcsec or 0.2 kpc at the distance of the source), were extracted from the shorter 12.8 ks data set. The emission from this region is dominated by the central AGN. The data for the four outer annuli (covering radii of 0.2-1, 1-4, 4-8 and 8-12 kpc, respectively) were extracted from the longer, full-frame observation. The spectra were grouped to contain a minimum of 20 counts per pulse invariant channel, allowing χ^2 statistics to be used. Background spectra were extracted from the blank-field data sets provided by the Chandra X-ray Center. Separate photon-weighted response matrices and effective area files were constructed for each region using the appropriate ACIS-S calibration and response files. We have used the ACISABS model in XSPEC to account for the time varying molecular contamination of the ACIS optical blocking filters.

The spectra have been analyzed using the XSPEC code (version 11.2.01; Arnaud 1996) and following the deprojection method described by Allen et al. (2001). We assume that the diffuse X-ray gas in each of the spherical shells, defined by the annuli mentioned above, is isothermal and can be described by a vmekal model (Kaastra & Mewe 1993; incorporating the Fe L calculations of Liedhal, Osterheld & Goldstein 1995) with the abundances of O, Mg, Si, S and Fe included as independent free fit parameters. The fit to the outermost annulus is used to determine the temperature, emission measure and abundances of the ISM in the outermost spherical shell. The contribution from that shell to each inner annulus is then determined by purely geometric factors. The fit to the second annulus is used to determine the parameters for the second spherical shell, and so forth, working inwards. For the central 2 arcsec region, we have included an additional power-law component to model the emission from the AGN (see Section 3). We assume that the intrinsic spectrum of the ISM in this region is the same as in the next annulus out. The emission from all annuli is assumed to be absorbed by a column density, N_{H} , of cold gas, which is a single, additional free parameter in the fits. The emission from the brightest knots of the jet and all other point sources were masked out and excluded from the analysis.

The deprojected temperature profile of the X-ray gas, determined from a simultaneous fit to the five annular regions, is shown by the solid points in Figure 2. The deprojected temperature decreases from $kT = 1.83 \pm 0.01$ keV at $r = 10$ kpc to $kT = 0.80 \pm 0.01$ keV within the central kpc (1σ errors). The total χ^2 for the deprojected fit of 3171 for 1271 degrees of freedom indicates that the simple, spherically-symmetric model provides an incomplete description of the Chandra data, which is unsurprising given the structural complexities evident in Fig. 1 (see also Wilson & Yang 2002 and Young et al. 2002). Nevertheless, the temperature measurements should provide a

reasonable description of the mean, emission-weighted properties in each spherical shell (although the uncertainties may be underestimated by a factor ~ 2). We note that the temperature measurement for the 0.2 – 1 kpc annulus is not affected significantly by flux from the central AGN, scattered outwards in the wings of the point spread function. In order to test this we carried out simulations in XSPEC, using our deprojected model, in which we added a power-law component to the model for the first annulus out (0.2-1kpc), with a strength calculated according to the observed nuclear flux and PSF models in the Chandra handbook. We find that the flux in the wings of the PSF has no significant effect on the best-fit parameters for the 0.2-1kpc annulus. To be conservative, we then doubled the strength in the wings and still found no significant change in the best-fit parameters, indicating that our results are robust against this effect.

Figure 2 also shows the importance of deprojecting the X-ray data when determining the central gas temperature (and hence the density profile). Without deprojection, we would infer a spuriously high temperature of $kT = 1.16 \pm 0.01$ keV for the 0.2 – 1.0 kpc region, which would impinge on the calculations of the accretion rate in Section 2.2. Note that deprojecting also improves the total χ^2 for the fit by 410 compared with a direct analysis of the projected spectra, without including additional free parameters in the fit.

The electron density profile for the X-ray gas, shown in Figure 2, was derived by deprojecting the surface brightness profile, given the deprojected temperature profile. At radii larger than a few kpc the density profile follows $\rho \propto r^{-1}$. Within the central ~ 2 kpc, the density profile flattens: fitting a constant value to the central two annuli we obtain $n_e = 0.170 \pm 0.003$ cm $^{-3}$ (or $n_e = 0.163 \pm 0.007$ cm $^{-3}$ for the innermost annulus).

2.2. \dot{M}

We can estimate the accretion rate from the ISM onto the central black hole using Bondi accretion theory; the nuclear accretion rate will thus be determined by the density and temperature of the hot gas at the point where the influence of the black hole becomes dominant. In the standard adiabatic problem (see Appendix A with $H = 0$ for the exact Bondi results), the Bondi (accretion) solution implies the sphere of influence of the black hole extends out to the gravitational capture radius (see also e.g.; Di Matteo et al. 1999; Quataert & Narayan 2000; Nulsen & Fabian 2000):

$$r_A \sim b \frac{GM}{c_s^2} = 0.05 T_{0.8}^{-1} M_9 \text{ kpc} \simeq 5 \times 10^5 r_{\text{Sch}}. \quad (1)$$

Here $M_9 = 10^9 M_\odot$ is the mass of the black hole ($M_9 = 3$), $T_{0.8} = T/0.8$ keV is the temperature in keV (cf. Figure 2), c is the speed of light, $c_s \sim 2.7 \times 10^7 T_{0.8}^{1/2}$ cm s $^{-1}$ is the sound speed (where T is the ISM gas temperature) and $r_{\text{Sch}} = 2GM/c^2$ is the Schwarzschild radius of the black hole. The parameter b depends on the detailed physics close to the accretion radius (including γ). We initially take $b \sim 1$, for which our definition of r_A corresponds to $\sim 2r_s$, the sonic radius of the black hole, and discuss this further in §5.1 and in the Appendix. Note that, depending on the

definition one chooses, r_A lies approximately at $0.5 - 2GM/c_s^2$. $r_A \gtrsim 0.2GM/c_s^2$ is resolved by *Chandra*.

Equation 1 shows that the accretion radius of M87 (for an assumed distance of 18 Mpc) corresponds to an angular scale of 2 arcsec. Thus, using *Chandra*, we are able to measure the properties of the gas at approximately the black hole accretion radius for M87. We note that the ionized disk of gas seen by HST (Harms et al. 1994) has been measured from 0.25 arcsec to about 2 arcsec from the nucleus, close to the Bondi radius of M87. HST, thus may have imaged the accretion flow in the optical I-band.

The accretion rate is related to the density and temperature at the accretion radius by the continuity equation:

$$\dot{M}_{\text{Bondi}} = 4\pi r_A^2 \rho_A c_s(r_A), \quad (2)$$

where ρ_A and $c_s(r_A)$ are the density and sound speed at the sonic radius. With the density and temperature measured directly at the accretion radius (Section 2.1), the Bondi accretion rate to M87 is given by

$$\begin{aligned} \dot{M}_{\text{Bondi}} &= 7 \times 10^{23} M_9^2 T_{0.8}^{-3/2} n_{0.17} \text{ gs}^{-1} \\ &\simeq 0.1 M_\odot \text{ yr}^{-1}. \end{aligned} \quad (3)$$

where $n_{0.17} = n/0.17 \text{ cm}^{-3}$. Eqn. (3) provides the accretion rate at the outer edge of the accretion flow. As discussed in Section 5, the mass accretion rate onto the black hole may be smaller if e.g. it decreases with radius because of an outflow (cf. Blandford & Begelman 1999).

The Bondi accretion rate (Eq. 3) implies a luminosity

$$L_{\text{Bondi}} = \eta \dot{M}_{\text{Bondi}} c^2 \simeq 5 \times 10^{44} \text{ erg s}^{-1} \quad (4)$$

if $\eta = 0.1$, as in a standard, radiatively efficient thin disk.

3. The X-ray Luminosity

The properties of the central AGN have been determined using the data for the central 2 arcsec (4 pixels) radius region after accounting for the emission from diffuse X-ray gas viewed in projection against the nucleus (see §2.1). We find that the central point source can be described by a power law model with a photon index $\Gamma = 2.23 \pm 0.04$ and a flux density at 1 keV of $(8.0 \pm 0.2) \times 10^{-13} \text{ erg cm}^{-2} \text{ s}^{-1} \text{ keV}^{-1}$ (1σ errors). We find no evidence for excess absorption associated with the central AGN ($\Delta N_{\text{H}} < 3.2 \times 10^{20} \text{ atom cm}^{-2}$ at 3σ confidence), over and above the mean value measured across the central 12 kpc radius region. We note that the mean absorbing column density measured across the central 12 kpc of $N_{\text{H}} = 1.97 \pm 0.12 \times 10^{20} \text{ atom cm}^{-2}$ is slightly lower than the nominal Galactic value of $2.5 \times 10^{20} \text{ atom cm}^{-2}$ determined from the HI studies of Dickey & Lockman (1990). This deficit may reflect residual systematic uncertainties in

the effective area of the instrument at low energies. Our results on the central AGN are in overall agreement with those of Wilson & Yang (2002; although these authors find a higher absorbing column density for the nucleus than the jet knots). Our measured photon index is slightly lower than the value of Marshall et al. (2001). (Note that our analysis differs from that of Wilson & Yang in that we account for the emission from diffuse X-ray gas viewed in projection against the nucleus.)

The observed nuclear luminosity is more than four orders of magnitude smaller than the predicted Bondi luminosity, implying (unless the Bondi estimate is inappropriate) that the radiative efficiency $\eta \sim 10^{-5}$. In the next section, we examine the predictions of hot accretion flow models with low radiative efficiencies.

4. Accretion models

A hot accretion flow around a supermassive black hole will radiate in the radio to X-ray bands. In the radio band, the emission results from synchrotron radiation. At higher energies, and up to the X-ray band, the emission is produced by bremsstrahlung processes and inverse Compton scattering of the soft synchrotron photons (e.g. Narayan, Barret & McClintock 1998).

In this Section, radii in the flow are written in Schwarzschild units: $r = ar_{\text{Sch}}$. We write black hole masses in solar units and accretion rates in Eddington units: $M_{\text{BH}} = mM_{\odot}$ and $\dot{M} = \dot{m}\dot{M}_{\text{Edd}}$. We take $\dot{M}_{\text{Edd}} = 10L_{\text{Edd}}/c^2 = 2.2 \times 10^{-8}mM_{\odot} \text{ yr}^{-1}$, i.e., with a canonical 10% efficiency. We take $a = 10^4$ to be the outer radius of the flow. The Bondi accretion rate for M87 in these units is $\dot{m}_{\text{Bondi}} = 1.6 \times 10^{-3}$.

The predicted spectrum from an ADAF depends (weakly) on the ratio of the gas to magnetic pressure β , the viscosity parameter α , and the fraction of the turbulent energy in the plasma which heats the electrons, δ . Here, we fix $\alpha = 0.1$, $\beta = 10$, and take $\delta = 0.3$ or 0.01. The two major parameters, though, are the accretion rate \dot{M} and the black hole mass M , both of which are constrained. With M given for M87, we normalize the models to the observed *Chandra* flux. This gives us the \dot{m} required by the models to explain the X-ray emission. A model is ruled out if it requires $\dot{m} \ll \dot{m}_{\text{Bondi}}$ to account for the observed luminosity or, equivalently, if we take $\dot{m} = \dot{m}_{\text{Bondi}}$ and the models predict a higher luminosity than is observed.

The solid dots in Figure 3 are the high resolution VLBI, HST, Gemini, Keck (at $10\mu m$) and *Chandra* high resolution measurements of the nuclear flux in the radio, optical, mid-infrared and X-ray bands, respectively. The open dots show the lower resolution VLA radio measurements which are likely to include a more significant contribution from the jet. The solid line shows the predicted spectrum for a pure inflow ADAF model adjusted to roughly match the 1 keV *Chandra* flux. In this model $\dot{m} = 6 \times 10^{-4}$, (with $\delta = 0.3$) which is consistent with the Bondi estimate (i.e. within the model uncertainties, which should be taken to be $\sim 50\%$). A model with $\delta = 0.01$ and a corresponding $\dot{m} = 10^{-3}$ is shown by the dotted line. The required accretion rates are always

large enough for Comptonization of the synchrotron emission to dominate the X-ray emission in these models (where the scattering optical depth in an ADAF is $\propto \dot{m}$; see e.g., Narayan et al. 1998). The exact positions of the Comptonization bumps in the optical and X-ray bands are a function of temperature and, therefore, δ . Models with higher values of electron heating, which are also preferred from a theoretical point of view, agree better with the measured 2–10 keV spectral slope of $\Gamma \sim 2.2$. Note that, as shown in Figure 3, the agreement with the observed spectrum is obtained only if the Compton bumps are pronounced, i.e. the agreement depends upon the details of the model.

Marshall et al. (2002) and Wilson & Yang (2002) have shown that the spectrum of the innermost jet knots observed by *Chandra* are consistent with that of the nucleus, possibly implying a similar origin. It is indeed plausible that a large fraction of the observed nuclear X-ray flux might be due to emission from the base of the jet⁶. The point of Figure 3 is to show that ADAF models are consistent with the requirement of a low-radiative efficiency. In fact, Figure 3 shows that it is possible for the accretion flow to account for a large fraction of the observed nuclear emission, thereby offering an alternative explanation.

5. Discussion

Chandra observations of the nucleus of M87 have resolved the properties of the ISM all the way into the Bondi radius of the central black hole. This makes M87 the only extragalactic black hole system in which both the gas temperature and density are measured into approximately the accretion region, and for which a Bondi accretion rate can be directly calculated (see Narayan 2002 or Quataert 2002 for similar study of Sgr A*). M87 also possesses a relatively bright nuclear source, the flux of which can be accurately measured in the X-ray band with *Chandra*, and throughout the whole of the spectral energy distribution with other observations. At present, M87 is the best constrained low-luminosity extragalactic black hole system. With both L_x and \dot{M} measured, we were able to show unambiguously that the black hole in M87 is highly underluminous with respect to its Bondi mass supply: the expected power output exceeds, by about 4 orders of magnitude, the observed value. If the black hole in M87 is indeed accreting close to its Bondi rate (cf., §5.1), the accretion efficiency, η , must be low. We have shown that the required values of η are consistent with predictions from ADAF models.

We note that our general result is independent of whether the observed nuclear luminosity is attributed to an ADAF or entirely dominated by jet emission (see e.g. Wilson & Yang 2002; Marshall et al. 2002). The constraints derived here show that it is possible for a significant fraction of the observed nuclear emission to be contributed by the accretion flow. More importantly,

⁶Note that it is not possible to put strong constraints on the nuclear variability from these two observations because of the different apertures considered in the published nuclear measurements. However, there does not seem to be evidence for substantial variability. Evidence for such variability would argue against simple ADAF models

perhaps, the requirement for low-radiative efficiency of the accreting gas can only be invalidated if the actual mass accreted by the black hole were to be a very small fraction of the mass supplied in the outer region of the flow (i.e. of \dot{M}_{Bondi}). This could be the case if strong outflows or perhaps convection are important in the accretion flow, as has been discussed by e.g. Blandford & Begelman (1999), Stone et al. (1999) and Quataert & Gruzinov (2000), Narayan et al. (2000), respectively (but see Balbus & Hawley’s [2002] discussion on convection). In such models, the accretion flow would produce a much lower luminosity than a pure inflow ADAF and make a negligible contribution to the observed luminosity (which, in the case of M87, can be easily explained by the jet emission. In the CDAF case, the energy would probably need to be tapped from the black hole’s spin in order to explain the high jet power). The Bondi rate could also be decreased if the jet heats the ISM. We discuss this further in §5.1.

In a previous study using radio observations, Di Matteo et al. (1999; 2000) favored outflow models for the nuclei of ellipticals. With *Chandra*, the properties of the central regions of the ISM gas have been determined more accurately for a number of elliptical galaxies (e.g., Loewenstein et al. 2001). In particular, the new observations have shown that the ISM density profiles tend to flatten off significantly in the central regions of ellipticals (as is the case in M87 - Figure 2), implying Bondi accretion rates smaller than was previously estimated. In most cases, *Chandra* does not detect nuclear point sources (Loewenstein et al. 2001). Given that their black hole masses are more uncertain, the constraints for these other low luminosity systems remain inconclusive. The only two *Chandra* detections of X-ray nuclear sources in low luminosity elliptical nuclei are in M87 and NGC 6166 (Di Matteo et al. 2001). For both of these nuclei, pure inflow ADAF models are consistent with the observational constraints and can explain large fractions of the observed nuclear fluxes. *Chandra* observations of Sgr A* have also measured the X-ray flux of the nuclear point source (Baganoff et al. 2001) and allowed us to estimate accretion rates onto the central black hole (e.g. Narayan 2002; Quataert 2002). Sgr A*, like the elliptical nuclei, also requires low radiative efficiency for the accreting gas and is consistent with ADAF models. Further constraints on ADAF and inflow/outflow models in the case of ellipticals will require knowledge of the contributions, over all wavelengths, of emission from the bases of the jets.

5.1. \dot{M}_{Bondi} , overall energetics and activity

Our fundamental conclusions rely on the assumption that the black hole in M87 is accreting mass at the Bondi rate. The predicted nuclear power of M87, for accretion at the Bondi rate, and $\eta = 0.1$ is $\sim 5 \times 10^{44} \text{ erg s}^{-1}$ (see Eq. 4). This estimate roughly matches some estimates of the kinetic power in the jet which is calculated to be $\approx 10^{44} \text{ erg s}^{-1}$ (e.g.; Bicknell & Begelman 1999; Owen et al. 2000; whereas Reynolds et al. 1996 obtain $\sim 10^{43} \text{ erg s}^{-1}$). A rough estimate of the jet power required to evacuate, at the sound speed, the inner cavities in the ICM associated with the inner radio lobes ($\simeq 2 - 3 \text{ kpc}$) in M87 implies $L_j \sim 3 \times 10^{42} \text{ erg s}^{-1}$ (Young et al. 2002). This value is smaller than the estimates of Bicknell & Begelman (1999) and Owen et al. (2000) but

only considers the cavities observed in the inner region of M87. Further, L_j would be higher if the cavities are evacuated supersonically.

We find, therefore, that the Bondi luminosity estimate roughly matches the overall energetics of the black hole in M87 (if this is indeed $\sim 10^{44}$ erg s $^{-1}$). This may provide support for the relevance of Bondi theory as a means of estimating the mass supply and the nuclear power of black holes in ellipticals. We note that the jet in M87 is also a low-efficiency radiator with a total bolometric luminosity of the order of 10^{42} erg s $^{-1}$ (Owen et al. 2000). Thus, based on these estimates of the power of the nucleus, the energy input if all the \dot{M}_{Bondi} reaches the black hole, at present dominates radiative losses from both the jet and accretion flow.

We discuss two alternative possibilities to the low-radiative efficiency scenario: (a) as mentioned above, Blandford & Begelman (see also e.g. Stone et al. 1999) have suggested that low luminosity accretion flows may develop strong outflows such that most of the mass and energy is removed from the accretion flows. In this case one may speculate that the accretion energy is emerging in the jet (it has been shown that the inner kiloparsec of M87 is highly magnetized and turbulent, e.g. Owen, Eilek & Keel 1990; Zhou 1998. Outflows may become collimated and radiate more efficiently when interacting with this medium). On the same note, Livio, Ogilvie & Pringle (1999) have argued that the energy extraction from black holes via MHD processes such as the Blandford-Znajek mechanism (Blandford & Znajek 1977) may in-fact be most efficient for advection dominated flows (see also Meier 2001).

(b) The central engine of M87 undergoes on-off activity cycles (e.g., Binney 1999; Owen et al. 2000). The black hole in M87 may have been active for 100-200 Myr (as derived from estimates of the current age of its radio halos; Owen et al. 2000). As long as the black hole is fed (e.g. at the estimated Bondi rate) it will have a strong effect on the ISM gas in the core (the bolometric X-ray luminosity of which is $\sim 10^{43}$ erg s $^{-1}$ in the inner 20 kpc or so; e.g. Nulsen & Böhringer 1995). The jet will disturb (or heat) the core regions, support bulk flows and turbulence. These extra pressure forces may, in turn, offset radiative cooling, support the gas against gravitational infall and suppress accretion onto the black hole (hence the jet activity itself). Once the central engine turns off, no energy is deposited in the core so that accretion at the standard Bondi rate and then jet activity resume.

The significant flattening of the X-ray gas density profile within the central 3 – 4 kpc (Fig. 2) may be a strong indication that indeed energy is being deposited in the central region of M87 (see also Loewenstein et al. 2001 for other Virgo ellipticals). A flat density profile can only arise if there is lots of mass dropout (see e.g.; Quatert & Narayan 2000) or maybe if gas is not flowing inward at all. Given that mass dropout is not seen in X-ray data at larger radii (Böhringer et al. 2002; Molendi & Pizzolati 2001) it is possible that something has affected the accretion radius and stifled accretion.

It is interesting to note that the mild peak in the Figure 2 density profile coincides with the ring at about 10 arcsec from the nucleus (Figure 1) which is also where the H- α emission peaks.

This possibly indicates that there could be stifled inflow within this radius and a cooling flow outside it. It is also notable that the few kpc radius corresponds approximately to the size of the inner radio lobes of M87 (Owen et al. 2000). There is also strong evidence of ‘cavities’ in the X-ray emitting gas of M87, the inner ones of which coincide with the inner radio lobes (Young et al. 2002; see also Fig. 1) and a number of other clusters containing radio galaxies (McNamara et al. 2000; Fabian et al. 2000; Heinz et al. 2002); some of these cavities are associated with observed radio lobes and others are hypothesized to be relics of old radio activity.

It has been shown that Bondi accretion can be significantly suppressed in a non-adiabatic gas (e.g. Ostriker et al. 1976). Following along these lines, we show that, at present, the energy dumped into the ISM by the jet in M87 may be sufficient to decrease the accretion rate with respect to the Bondi value by a factor $\lesssim 10^6$. We do not attempt to build a detailed model but just qualitatively discuss the implications of non-adiabatic Bondi accretion for M87.

We consider a jet of power L_j and velocity v_j advancing into the ISM with density ρ . The jet forces its way outwards at a speed v_h which is obtained by balancing the outward momentum flux of the jet with the pressure of the ISM. As long as v_h is larger than the sound speed c_s in the ISM, the thermal pressure will be dominated by the contribution ρv_h^2 from ram pressure. Hence $v_h \sim (L_j/\rho A_h v_j)^{1/2}$. When v_h no longer exceeds c_s , the jet will slow down and dump energy in the surrounding medium. The inner radio lobes (in the inner few kpc) in M87 may be associated with such a region. Recent *Chandra* observations of M87 (Young et al. 2002) and other radio galaxies in clusters show no evidence that such interactions lead to sharp bow-shock regions. More often, it seems that jets are responsible for inflating bubbles in the surrounding ISM which then expand buoyantly (i.e. roughly at the sound speed; e.g. Churazov et al. 2001; Reynolds, Heinz & Begelman 2002) and give rise to radio lobes and corresponding X-ray structures. We take πr^2 to be the cross sectional area of the bubble inflated by the jet around the centre (which, for simplicity, we take to be spherical see e.g. Churazov et al. 2001; Reynolds et al. 2002)

Taking the mass, momentum and adding the energy conservation equation to the standard Bondi problem one can solve for the accretion radius (see details in Appendix A) with the addition of an energy (heat) source. In this case the accretion radius is reduced to:

$$r_s = \frac{GM}{2c_s^2} - \frac{2}{3} \frac{r_s^2}{c_s^3} (H), \quad (5)$$

where the heating is in units of $\text{erg s}^{-1} \text{g}^{-1}$ and the first term in Equation 5 is the standard Bondi radius as in Equation 1. According to the considerations above we write the energy deposited by the jet as: $H = L_j/m$ (where m is the total gas mass) with $L_j \sim \pi r^2 \rho v_j v_h^2$ so that $H \sim v_j v_h^2/r$. In this problem we take heating (i.e., the energy deposition) to be occurring around the accretion radius of the black hole (see Appendix for details). The inner radio lobes and X-ray cavities both on kpc scale may be indications that this is not too bad an approximation (although these are at radii which are more than an order of magnitude larger than the accretion radius). The resulting

accretion radius will rescale from the classical Bondi value roughly as,

$$r_s \sim \frac{GM}{c_s^2} \left(\frac{v_j}{c_s} \right)^{-1} \quad (6)$$

where we have assumed that $v_h \sim c_s$, the velocity of the bubble inflated by the jet in the ISM. Equation 6 clearly shows that the if bulk motions (as well as heat) at speeds $> c_s$ are created by the jet, then the accretion rate is affected.

The flow velocity of the M87 jet on scales of a few hundred parsec is highly relativistic (Biretta, Zhou & Owen 1995). Thus, according to the above scaling the accretion radius of M87 is likely to be reduced by a factor $\sim 1,000$. This would imply a decrease in mass accretion rate by $\sim 10^6$. This is more than enough to relax the requirement for low-radiative efficiency of the accreting gas. This may also provide support for the idea that the engine of M87 may undergo cycles of activity and at present the black hole is accreting at rates much lower than the Bondi rate. However, the transit time from the nucleus to the knot A in the jet (at a distance of ~ 1 kpc) is only about ~ 3000 yrs. This implies that for the accretion rate to be low now, the last active phase must have been a "burst-like" event of strong accretion on a relatively short timescale.

We thank Eliot Quataert for comments on the manuscript. T.D.M. acknowledges support for this work, while at CfA, provided by NASA through Chandra Postdoctoral Fellowship grant number PF8-10005 awarded by the Chandra Science Center, which is operated by the Smithsonian Astrophysical Observatory for NASA under contract NAS8-39073 and for grant NAG-10105. ACF and SWA acknowledge the Royal Society. This work was also supported by NASA through grants NAG 81755 and NAG 81027 to the University of Maryland.

REFERENCES

- Allen S.W., Etori S., Fabian A.C., 2001, MNRAS, 324, 877
- Arnaud, K.A., 1996, in *Astronomical Data Analysis Software and Systems V*, eds. Jacoby G. and Barnes J., ASP Conf. Series volume 101, p17
- Baganoff et al., 2001, ApJ, submitted (astro-ph/0102151)
- Balbus A.S., Hawley J.F., 2002, ApJ, 573, 749
- Bicknell, G.V., Begelman, M.C., 1999, in *The Radio Galaxy Messier 87*, ed. Roser, H.J., & Meisenhaimer, K., (Berlin: Springer), p. 235
- Binney, J.J., 1999, in *The Radio Galaxy Messier 87*, ed. Roser, H.J., & Meisenhaimer, K., (Heidelberg: Springer), p. 136
- Biretta J.A., Zhou, F., Owen F., 1995, ApJ, 447, 582
- Biretta J. A., Stern C. P., Harris D. E., 1991, AJ, 101, 1632

- Blandford R.D., Begelman M.C., 1999, MNRAS, 303, L1
- Blandford, R.D. & Znajek, R.L., 1977, MNRAS, 179, 433
- Böehringer, H., Matsushida, K., Churazov E., Ikebe Y., Chen Y., 2002, A&A, 482, 804
- Churazov, E., Brüggem, M., Kaiser, C. R., Böhringer, H., & Forman, W. 2001, ApJ, 554, 261
- Dickey J.M., Lockman F.J., 1990, ARA&A, 28, 215
- Di Matteo T., Fabian A.C, Rees M.J., Carilli C., Ivison R J., 1999, MNRAS, 305, 49
- Di Matteo, T., Quataert, E., Allen, S.W., Narayan, R., Fabian, A. C., 2000, MNRAS, 311, 507
- Di Matteo, T., Johnstone, R.M., Allen S.W., Fabian A.C., 2001, ApJ, 550, L19
- Fabian et al., 2000, MNRAS, 318, L65
- Ferrarese, L., Merritt, D., 2000, ApJ, 539, L9
- Ford H. C. et al. 1995, ApJ, 1994, 435, L27
- Harms R. J. et al., 1994, ApJ, 435, L35
- Heinz S., Choi Y., Reynolds C.S., Begelman M., 2002, ApJ, 569, L79
- Kaastra J.S., Mewe R., 1993, Legacy, 3, 16, HEASARC, NASA
- Liedhal D.A., Osterheld A.L., Goldstein W.H., 1995, ApJ, 438, L115
- Livio M., Ogilvie G.I., Pringle J.E., 1999, ApJ, 512, 100
- Loewenstein, M., Mushotzky, R. F., Angelini, L., Arnaud, K. A., & Quataert, E. 2001, ApJ, 555, L21
- Magorrian, J. et al. 1998, AJ, 115, 2285
- Marshall, H., Miller, B.P., Davis, D.S., Perlman E.S., Wise M., Canizares C.R., Harris, D.E., 2002, ApJ, 564, 683
- Meier D.L., 2001, ApJ, 548, L9
- McNamara et al., 2000, ApJ, 534, L135
- Molendi, S., Pizzolato, F., 2001, ApJ, 540, 194
- Narayan R., 2002, to appear in "Lighthouses of the Universe" eds. M. Gilfanov, R. Sunyaev et al., Springer-Verlag; Garching, 2001
- Narayan R., Yi I., 1995, ApJ, 444, 231
- Narayan R., Barret D., McClintock J., 1997, ApJ, 482, 448
- Narayan R., Igumenshchev, I. V. Abramowicz, M. A., 2000, ApJ, 539, 798
- Nulsen, P.E.J., Böehringer, H., 1995, MNRAS, 274, 1093
- Nulsen, P.E.J., Fabian, A.C., 2000, MNRAS, 311, 346
- Ostriker, J. P., Weaver, R., Yahil, A., & McCray, R. 1976, ApJ, 208, L61

- Owen F.N., Eilek J.A., Kassim N. E., 2000, ApJ, 543, 611
- Owen F.N., Eilek J.A., Keel, W.C., 1990. ApJ, 362, 449
- Pauliny-Toth I. I. K., Preuss E., Witzel A., Graham D., Kellerman K. I., Ronnang B., 1981, AJ, 86, 371
- Perlman E.S., Sparks W.B., Radomski J., Packham C., Fisher R.S., Pina R., Biretta J.A., ApJ, 561, L51
- Quataert E., 2002, ApJ, 575, 855
- Quataert E., Gruzinov I., 2000, ApJ, 539, 809
- Quataert E., Narayan R., 2000, ApJ, 528, 236
- Reid M. J., Biretta J. A., Junor W., Muxlow T. W. B., Spencer R. E., 1989, ApJ, 336, 112
- Reynolds C. S., Di Matteo T., Fabian A. C., Hwang U., Canizares C. R., 1997, MNRAS, 283, L111
- Reynolds C. S., Heinz S., Begelman M., 2002, MNRAS, 232, 271
- Stone, J. M., Pringle, J. E. Begelman, M. C. 1999, MNRAS, 310, 1002
- Wilson, A. S. & Yang, Y. 2002, ApJ, 586, 133
- Young A.J., Wilson A.S., Mundell C.G., ApJ, in press
- Zhou, F., Ph.D. thesis, New Mexico Tech.

A. Appendix

In order to show the effects of a jet of power L_j dumping its energy in the ISM gas, we write the mass, momentum and energy conservation equations for the accretion radius under the conditions of spherically symmetric, steady ($\partial/\partial t = 0$) accretion. We consider the most of the heating to be occurring within or just outside the accretion radius.

$$\dot{M} = 4\pi r^2 \rho(r)v(r), \tag{A1}$$

$$v \frac{dv}{dr} + \frac{1}{\rho} \frac{dP}{dr} + \frac{GM}{r^2} = 0 \tag{A2}$$

and

$$v \frac{d}{dr} \left[\frac{v^2}{2} + (\gamma - 1) \frac{P}{\rho} \right] = -\frac{GM}{r^2} v + H \tag{A3}$$

where the quantities \dot{M} , ρ , v , P and γ represent the mass accretion, the mass density, the radial velocity, the pressure, the gas adiabatic index, respectively. H is the heating rate. Using (A1) and

taking $\gamma = 5/3$ we rewrite Eqs. (A2) and (A3) as

$$\begin{aligned} \frac{dv}{dr} \left(\frac{v^2}{c_s^2} - 1 \right) &= -\frac{GMv}{r^2 c_s^2} - \frac{2H}{3c_s^2} - \frac{2v}{r} \\ \frac{3}{2} \frac{dc_s^2}{dr} \left(\frac{v^2}{c_s^2} - 1 \right) &= \frac{GM}{r^2} - \frac{2v^2}{r} + \frac{5v^2 - 3c_s^2}{3c_s^2 v} H \end{aligned} \quad (\text{A4})$$

For the flow to satisfy the appropriate boundary conditions, $v \rightarrow 0$ as $r \rightarrow \infty$ and $v \rightarrow (GM/r)^{1/2}$ as $r \rightarrow 0$, the two equations above must have a sonic point at $r = r_s$ where $v^2 = c_s^2$. The only solutions that are continuous imply that the RHS of both equations is 0. Both equations have the same sonic radius, and solving for that gives,

$$r_s = \frac{GM}{2c_s^2} - \frac{2}{3} \frac{r_s^2}{c_s^3} (H), \quad (\text{A5})$$

where the heating and cooling rates are in units of $\text{erg s}^{-1} \text{g}^{-1}$. The factor 2/3 applies to the $\gamma = 5/3$ case but can be substituted (and thus generalized) by the term $(\gamma - 1)$.

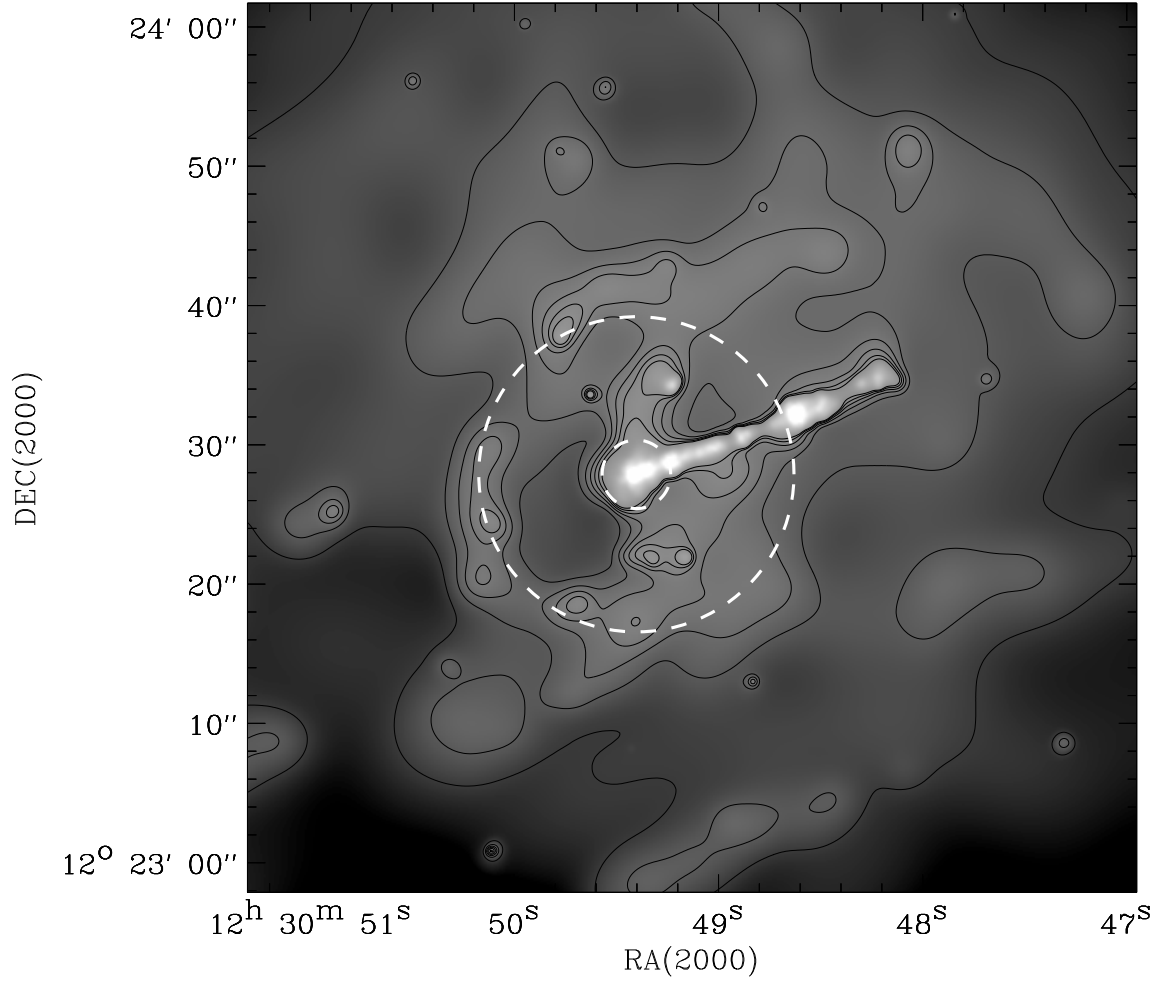


Fig. 1.— *Chandra* image of M87 and the core of the Virgo cluster in the 0.5 – 5 keV energy band. Overlaid are 8 logarithmically spaced contours from 5 – 30 counts per $0''.5$ pixel (solid lines) and the inner annulus used for the deprojection analysis (white dashed circles, centered on the nucleus). The image has been adaptively smoothed so that the signal-to-noise ratio of the signal under the smoothing kernel at each point on the image is at least 3.

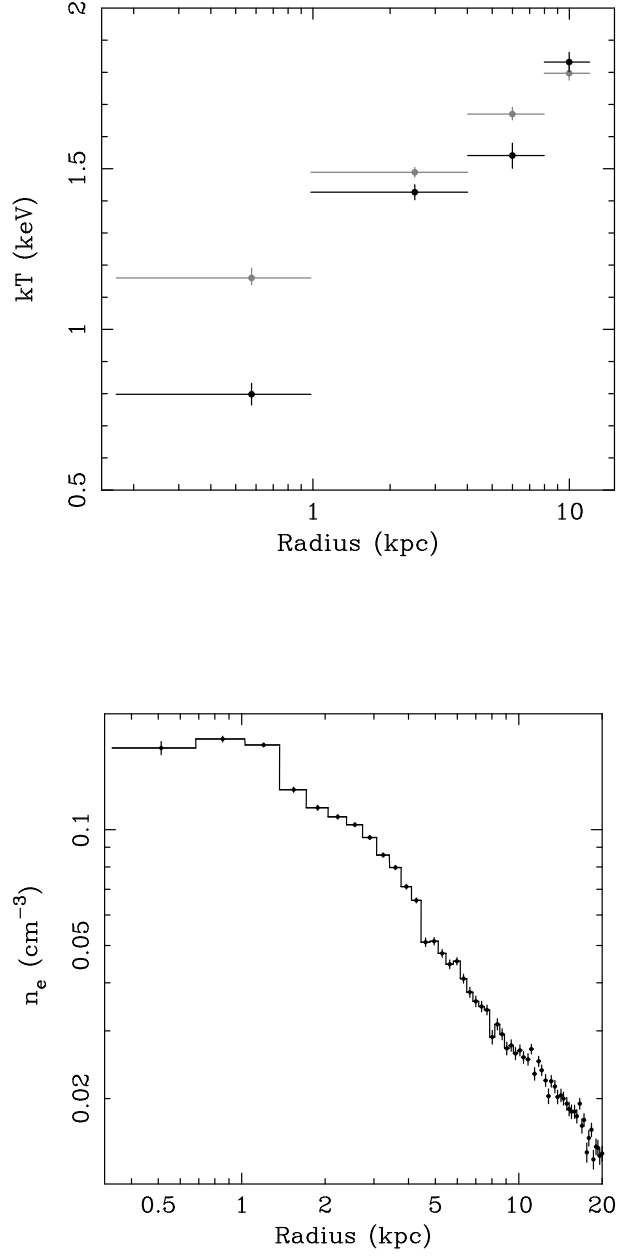


Fig. 2.— Top: The temperature profile of the ISM in M87 measured by *Chandra*. The dark points show the deprojected temperature measurements and the grey ones the observed (projected) values. The 1σ error bars have been multiplied by a factor of 3 to improve their visibility. Bottom: The (electron) density profile of the ISM. Error bars are the 1σ uncertainties.

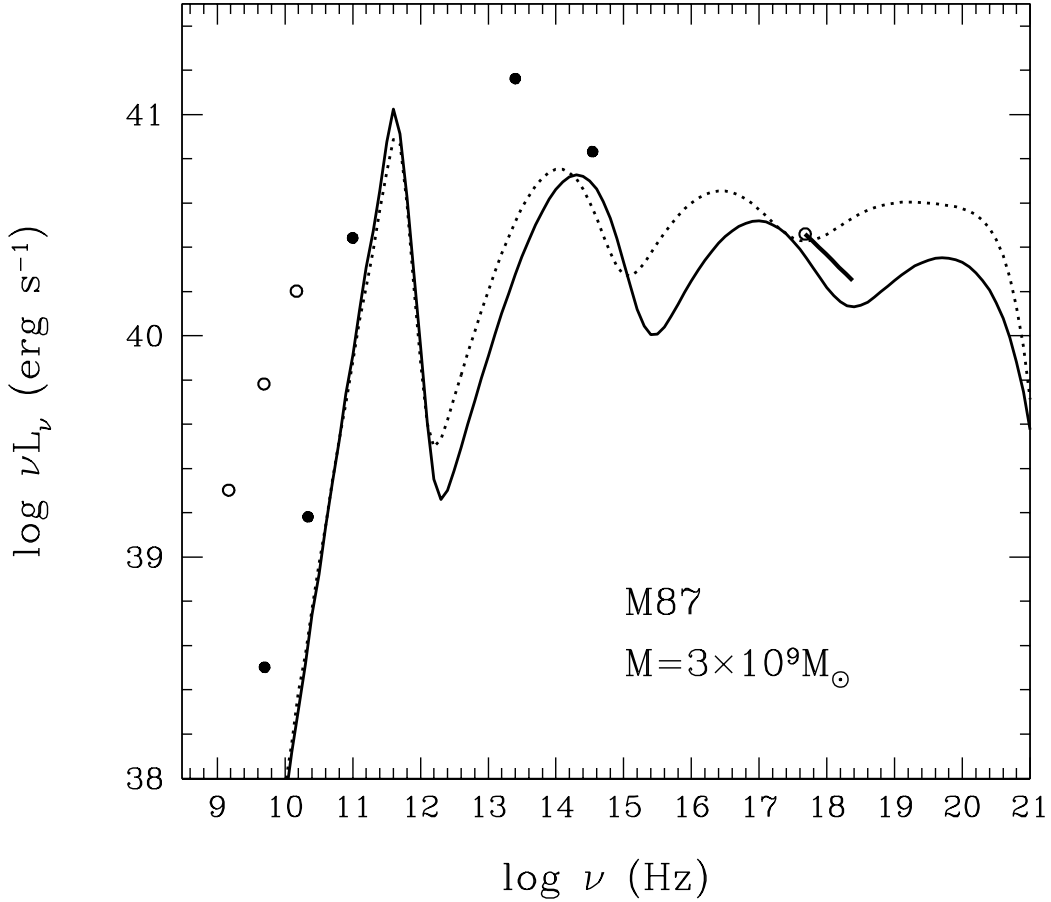


Fig. 3.— Spectral models calculated for hot accretion flows normalized to the *Chandra* X-ray flux. The solid line is an ADAF model with $\delta = 0.3$. The required accretion rate, $\dot{m} = 7 \times 10^{-4}$, is consistent with the Bondi value. The dotted line shows a model with $\delta = 0.01$ with $\dot{m} = 10^{-3}$. The filled dots are the VLBI nuclear flux density measurements by Paulini-Toth et al. (1981); Spencer & Junor (1986) and Bääth et al. (1992) in increasing frequency order, respectively. The IR, 10 μ m nuclear flux measurement is the best IR nuclear flux limit (resolution of ~ 0.46 arcsec) from Gemini (Perlman et al. 2001). The optical nuclear continuum measurement (also a filled dot) is from HST (which has resolution of 0.15 arcsec) observations by Harms et al. (1994). The open circles are lower resolution measurements by Biretta et al. (1991). The radio and optical data are tabulated by Reynolds et al. (1996). The thick solid line shows the *Chandra* spectrum (in the 0.2 – 10 keV band).